Available online at www.sciencedirect.com
ScienceDirect
Trans. Nonferrous Met. Soc. China 35(2025) 2008−2020
Transactions of Nonferrous Metals Society of China
www.tnmsc.cn

Suppression of Ag dewetting and sinterability improvement of submicron Ag-coated Cu particles as fillers in sintering paste by surface modification with stearic acid

Yeongjung KIM[1], Yong-Sung EOM[2], Kwang-Seong CHOI[2], Jong-Hyun LEE[1,3]

1. Department of Materials Science and Engineering, Seoul National University of Science and Technology, 232 Gongneung-ro, Nowon-gu, Seoul 01811, Korea;
2. Low-Carbon Integration Tech, Creative Research Section, ETRI, 218 Gajeong-ro, Yuseong-gu, Daejeon 34129, Korea;
3. Materials Research Institute for Future Convergence, Seoul National University of Science and Technology, 232 Gongneung-ro, Nowon-gu, Seoul 01811, Korea

Received 18 October 2023; accepted 27 May 2024

Abstract: Four types of submicron Ag-coated Cu particles with different Ag contents were prepared as sintering paste fillers, and the Ag contents of the particles were measured to be 10, 20, 30, and 40 wt.%. Four types of particles (in order of increasing Ag content: A10, A20, A30, and A40) were surface-modified with stearic acid, to suppress the Ag shell dewetting and improve sinterability. The surface-modified particles were mixed with a polyol-based solvent to fabricate a resin-free paste. Subsequently, the pastes were screen-printed onto a slide glass and sintered at 250 °C in a nitrogen atmosphere for 1−10 min to form an electrode. The electrical resistivity of the sintered film as a function of sintering time was measured using a four-point probe. All the four surface-modified Cu@Ag particles with different Ag contents exhibited decreased electrical resistivity. Particularly, the largest difference in values after and before the surface modification was observed for A40 with the highest Ag content; the electrical resistivities of the initial and surface-modified particles were 1.51×10^{-4} and 6.67×10^{-5} Ω·cm, respectively, after sintering for 10 min. The findings of this study confirmed that the surface modification using stearic acid effectively suppressed the dewetting of the Ag shell and improved the sinterability of the submicron Cu@Ag particles.

Key words: submicron Ag-coated Cu particle; sintering; dewetting; surface modification; stearic acid; electrical resistivity

1 Introduction

In contrast to conventional lithography, low-cost and eco-friendly additive methods such as inkjets, screens, and roll-to-roll printing are widely used to manufacture electrodes and conductive films on flexible substrates [1−4]. Different sintering processes, such as thermal sintering, laser sintering, and intense pulsed light (IPL) sintering, have been introduced as post-processing treatments after printing [5−9]. Thermal sintering using sintering paste is currently the most common method because numerous samples can be manufactured, and a large-area film can be formed simultaneously, leading to high productivity [10,11]. Owing to their excellent electrical and thermal conductivities, copper and silver are used as representative fillers for sintering pastes [12,13]. Cu is a low-cost material; however, it is easily oxidized in air, and the oxidation is accelerated at high temperatures [14,15]. By contrast, Ag has excellent

Corresponding author: Jong-Hyun LEE, Tel: +82-2-970-6612 (office), +82-10-2214-4974 (mobile), E-mail: pljh@snut.ac.kr
https://doi.org/10.1016/S1003-6326(25)66797-5

oxidation resistance but is expensive [16,17].

Therefore, Ag-coated Cu (Cu@Ag) core–shell particles, which exhibit excellent antioxidation properties and are price competitive, have attracted growing attention and are actively researched worldwide [18−21]. Several researchers have evaluated the electrical properties of conductive films sintered using pastes and ink containing Cu@Ag particles [22−24]. For example, YU et al [25] manufactured a conductive ink containing Cu@Ag nanoparticles and evaluated its electrical resistivity. The electrical resistivity was measured to be $1.03\times10^{-4}\,\Omega\cdot$cm when the film was sintered for 60 min at 250 °C in a reductive atmosphere [25]. However, Cu@Ag nanoparticles are expensive to fabricate and store owing to their low yields and interparticle aggregation, respectively [26−29]. In addition, preparing a paste with uniformly dispersed fillers using nanoparticles is difficult, limiting their commercial use [30]. ZHANG et al [31] obtained an excellent electrical resistivity of $6.39\times10^{-6}\,\Omega\cdot$cm when cured at 200 °C for 60 min using a resin-based electrically conductive adhesive containing micron Cu@Ag particles, but the value was $4.09\times10^{-4}\,\Omega\cdot$cm when measured after curing for 30 min. Hence, resin-based pastes exhibit excellent electrical conductivity but require long sintering time, which reduces their productivity [32,33].

Contrary to expectations that Cu@Ag particles would exhibit excellent oxidation resistance, core Cu is oxidized by out-diffusion when heated in air, and oxidation is further accelerated by dewetting of the Ag shell due to lattice mismatch between Cu and Ag at temperatures higher than 200 °C [34−36]. This significantly degrades the sinterability, and countermeasures have not yet been adequately studied.

Therefore, authors have conducted a study on surface modification of Cu@Ag particles using three types of dicarboxylic acids to suppress Ag dewetting and improve sinterability by reducing the surface energy [37]. The pristine Ag shell tends to dewet and transform into spherical particles on the unstable interface with core Cu due to lattice mismatch and so on [34−36], However, the dewetting and agglomeration of Ag shell can be suppressed with the reduced surface energy of Ag shell by the surface modification even if the interface instability is still identical [37]. It was verified that Ag dewetting was suppressed by formation of organometallic surface, and the effectiveness varied depending on the type of carboxylic acid used for surface modification. However, the difference in the effectiveness of surface modification and Ag dewetting suppression depending on the Ag shell thickness of Cu@Ag particles was not confirmed.

In this study, submicron-size Cu@Ag particles that are easy to precisely control the Ag shell thickness compared to micron-size particles were used as the filler material in a binder-free conductive paste to achieve both high packing density and easy mixing during paste preparation. The surface modification was performed using a stearic acid, a fatty acid with large molecular weight and long-chain structure different from those of dicarboxylic acids, to verify the suppression degree of Ag dewetting when using different acids with one carboxyl group, and four types of Cu@Ag particles with different Ag shell thicknesses were evaluated to find differences in the suppression behavior of Ag dewetting and sinterability increment. Pastes containing the surface-modified Cu@Ag particles were screen-printed onto a slide glass to form films. After sintering in a nitrogen atmosphere, the electrical resistivity of a sintered film was measured to quantitatively compare the sinterability.

2 Experimental

2.1 Ag coating and surface modification

The submicron Cu particles used for the Ag coating were synthesized using a wet chemical method, and their average diameter was ~350 nm. After synthesis, the Cu particles dispersed in the colloid were rinsed four times by centrifugation at 7000 r/min using ethanol and then dried for 6 h in a vacuum chamber at 25 °C. The obtained Cu powders were dispersed in 100 mL of deionized (DI) water to prepare a Cu colloid, and then Ag coating solutions with different amounts of the Ag precursor were added drop wise at a rate of 5 mL/min to fabricate four types of particles with Ag contents of 10, 20, 30, and 40 wt.% (A10, A20, A30, and A40, respectively). The Ag coating solution was prepared by sequentially dissolving 5 mol/L sodium hydroxide (NaOH, 98%, Samchun Chemicals), 1.25 mol/L EDTA ($C_{10}H_{16}Na_2O_8$, 98.5%, Yakuri Pure Chemicals), and 0.16 mol/L

silver nitrate ($AgNO_3$, 99.99%, Hojeonable Inc.) in DI water. The solution was stirred at 300 r/min for 30 min to form a uniform Ag shell via the galvanic replacement reaction. Cu@Ag particles dispersed in the colloid were rinsed by centrifugation using DI water and ethanol and then dried for 6 h in a vacuum chamber at 25 °C.

Four types of Cu@Ag particles fabricated with different Ag contents were surface-modified by immersion in an acidic solution. The acidic solution was prepared by dissolving 0.1 mol/L stearic acid ($C_{18}H_{36}O_2$, 95%, Duksan Pure Chemicals), a type of fatty acid having long alkyl chains, in 100 mL of ethanol at room temperature (25 °C). The Cu@Ag particles were then dispersed in the solution and stirred for 1 min. Thereafter, the solution was ultrasonicated for 30 min to facilitate the surface modification. The surface-modified Cu@Ag particles were rinsed and decanted thrice using ethanol and then dried for 6 h in a vacuum chamber at 25 °C. Figure 1 shows a schematic illustration of the Ag coating fabrication and surface modification process.

2.2 Paste preparation and film formation

The pastes were prepared by mixing each of the four initial and surface-modified Cu@Ag particles with a polyol-based solvent (EW10, Epsilon Epowder) at a particle/solvent mass ratio of 75:25. The prepared pastes were screen-printed onto a slide glass with a volume of 5 mm × 5 mm × 0.1 mm using a stencil mask and squeegee, and the printed films were sintered at 250 °C for 1−10 min in a nitrogen atmosphere. The samples placed in a furnace were heated to 250 °C at an average heating rate of 50 °C/min with nitrogen purge at a flow rate of 100 mL/min. The sintering time was determined by timing from when the temperature reached 250 °C. The samples were cooled in a furnace with the continuously injected nitrogen at a flow rate of 200 mL/min after the sintering time elapsed and taken out. Figure 2 shows a schematic diagram of the paste preparation and sintering processes.

2.3 Characterization

The surface morphologies of the initial and surface-modified submicron Cu@Ag particles and

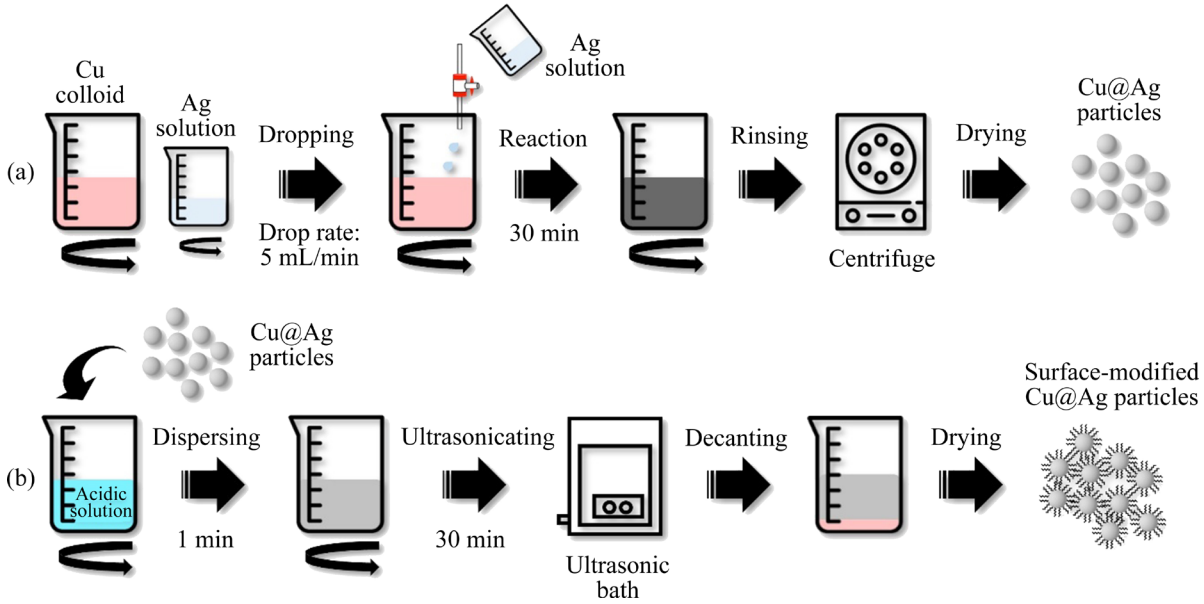

Fig. 1 Schematic diagrams of fabrication of Ag coating (a) and surface modification process (b) of submicron Ag-coated Cu particles

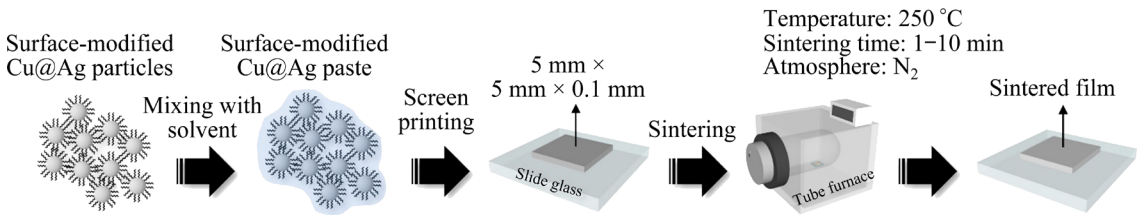

Fig. 2 Schematic diagram of sintering process using surface-modified submicron Ag-coated Cu particles

changes in the microstructure of the sintered film were observed using high-resolution field emission scanning electron microscope (HRFE-SEM, SU8010, Hitachi). Ag contents of the four types of Cu@Ag particles were measured using inductively coupled plasma optical emission spectroscopy (ICP-OES, 5100 SVDV, Agilent). Changes in the phase of Cu@Ag particles before and after surface modification were analyzed using X-ray diffraction (XRD, SmartLab, Rigaku) with Cu K_α radiation (λ=1.54 Å) at a scanning rate of 0.2 (°)/s in a 2θ range of 10°−80°. Fourier transform infrared spectroscopy (FT-IR, 670, Varian) and X-ray photo-electron spectroscopy (XPS, Nexsa, ThermoFisher) were performed to detect the carboxylate ligands on the Ag shell surface and binding states of the surface-modified Cu@Ag particles, respectively. Thermogravimetry differential thermal analysis (TG−DTA, DTG−60H, Shimadzu) was conducted to confirm the thermal properties and Ag dewetting behavior of the pastes containing surface-modified Cu@Ag particles; the mass change and heat input/output owing to the reaction were measured by heating at a rate of 20 °C/min up to 350 °C in the dynamic heating mode. In addition, the thermal decomposition reaction of ligands was analyzed by heating at a rate of 30 °C/min up to 250 °C, which was followed by maintaining for 20 min in the isothermal heating mode. The sinterability of the surface-modified Cu@Ag particles was evaluated by measuring the electrical resistivities of the sintered films using a four-point probe connected to a source meter (2400, Keithley). The resistivity values were presented as the average and standard deviation calculated from the results of ten measurements.

3 Results and discussion

3.1 Characteristics of submicron Cu@Ag particles

Figure 3 shows the surface morphologies of the submicron Cu@Ag particles fabricated with different Ag contents. The average particle sizes were maintained to be ~350 nm after Ag coating, and the Ag contents were 10, 20, 30, and 40 wt.% as measured using ICP-OES, which showed an increase with increasing amounts of Ag precursor added during Ag coating. Rough surfaces owing to nodules with tens of nanometers in size were observed as Ag shells were formed, which became more pronounced with increasing Ag content. This is due to the gradual growth of nodules formed on the surface during the initial stage of the coating reaction by the reduction of the Ag−EDTA complexes. The average nodule sizes were 17, 22, 30, and 43 nm for A10, A20, A30, and A40,

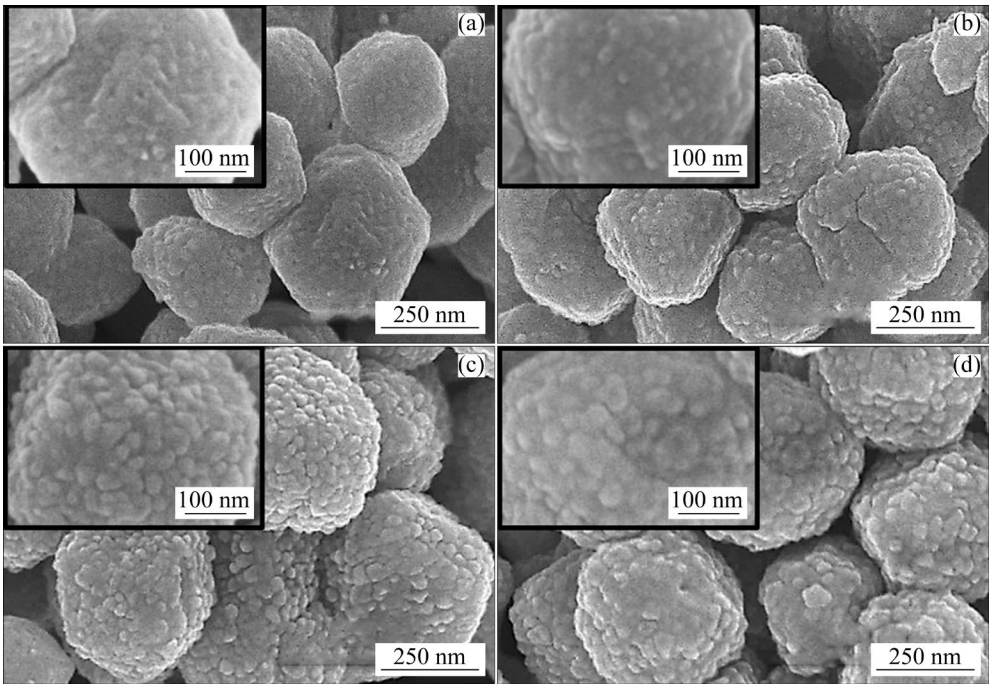

Fig. 3 High- (inset) and low-magnification SEM images of pristine submicron Ag-coated Cu particles with different Ag contents: (a) 10 wt.%; (b) 20 wt.%; (c) 30 wt.%; (d) 40 wt.%

respectively, confirming that the size of the nodules gradually increased with increasing Ag content. In addition, no particle aggregation occurred during the Ag-coating reaction or drying.

Figure 4 shows the cross-sectional backscattered electron (BSE) images of the submicron Cu@Ag particles fabricated with different Ag contents. The Ag shells surround the core Cu, indicating a core–shell structure, and are formed with uniform thickness owing to the stable galvanic displacement reaction. The thickness of Ag shells increased with increasing Ag content; for A10, A20, A30, and A40, the average thicknesses were 6.94, 14.70, 22.84, and 32.41 nm, respectively (Fig. 4(e)). The growth mechanism of Ag shells is believed that interdiffusion of Cu atoms outward and Ag atoms inward makes the core Cu atoms penetrate the just formed single-atomic-layer Ag shell and encounter external Ag−EDTA complexes in the solution, forming an additional Ag layer by another galvanic reaction, which can be termed self-limiting shell formation [38]. Accordingly, the sinterability of the Cu@Ag particles is expected to vary depending on the Ag content and thickness of the Ag shell.

3.2 Surface modification of Cu@Ag particles

Figure 5 shows the changes in the surface morphology of the submicron Cu@Ag particles surface-modified with stearic acid. The surfaces of all four types of Cu@Ag particles with different Ag contents became relatively smooth after surface modification. This was owing to the neighboring

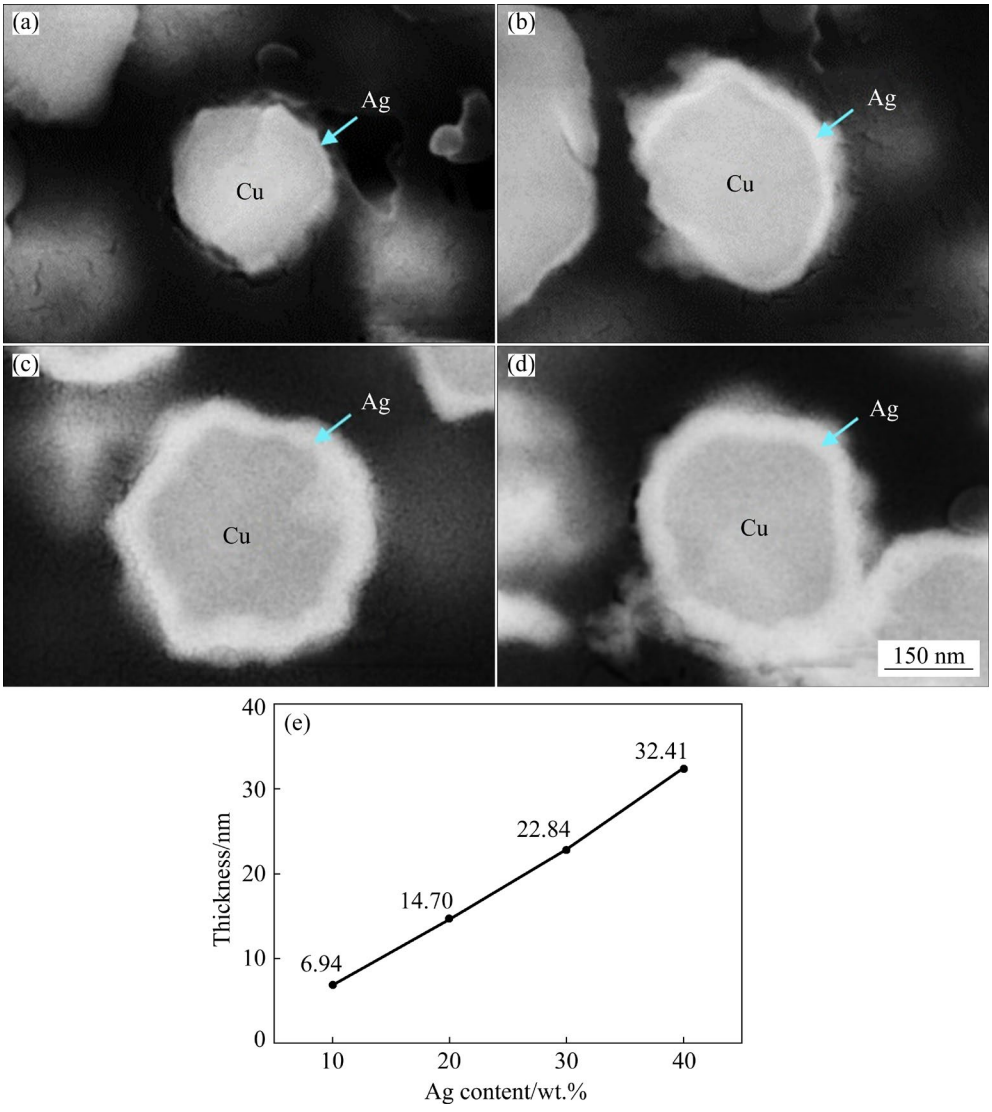

Fig. 4 Cross-sectional BSE images of submicron Ag-coated Cu particles with different Ag contents of 10 wt.% (a), 20 wt.% (b), 30 wt.% (c), and 40 wt.% (d), and thicknesses of Ag shells in submicron Ag-coated Cu particles with different Ag contents (e)

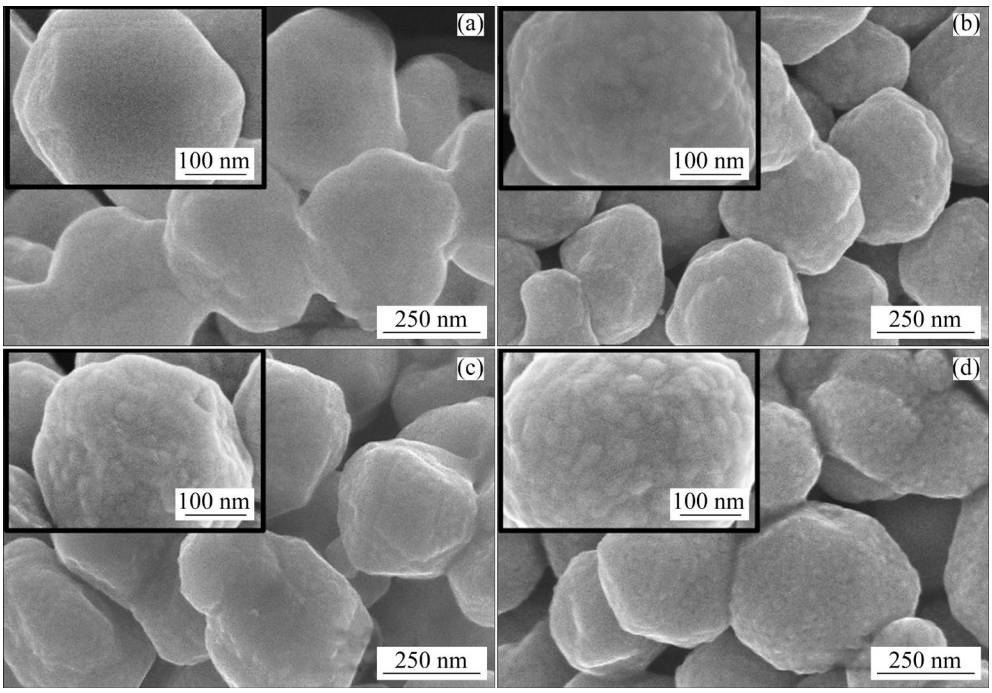

Fig. 5 High- (inset) and low-magnification SEM images of surface-modified submicron Ag-coated Cu particles with Ag contents of 10 wt.% (a), 20 wt.% (b), 30 wt.% (c), and 40 wt.% (d)

nodules that fused together and coarsened because an organometallic surface (COO—Ag) was formed by carboxylate ligands ($RCOO^-$), as reported in our previous research [37]. The decrease in the surface roughness varied depending on the Ag content. For A10, which had the thinnest Ag shell and smallest nodules of ~17 nm in size among the four types of particles, the nodules were removed entirely, and a smooth surface was observed (Fig. 5(a)). However, in the case of A40, which had the thickest Ag shell and biggest nodules of ~43 nm in size, the nodules were not completely coarsened and their shape remained even after surface modification.

Figure 6 shows the XRD patterns of the initial and surface-modified submicron Cu@Ag particles with different Ag contents. For all the particles, peaks corresponding to the (111), (200), and (220) planes of Cu and (111), (200), (220), and (311) planes of Ag were detected, and the intensity of the peaks due to Ag increased with increasing Ag content. No other phases, such as Cu oxides or hydroxides, were formed for initial Cu@Ag particles during the Ag coating process. Meanwhile, no changes in the diffraction patterns were detected after surface modification, indicating that no salts, such as silver stearate, were formed. Therefore, the carboxylates were bonded to Ag atoms in the form

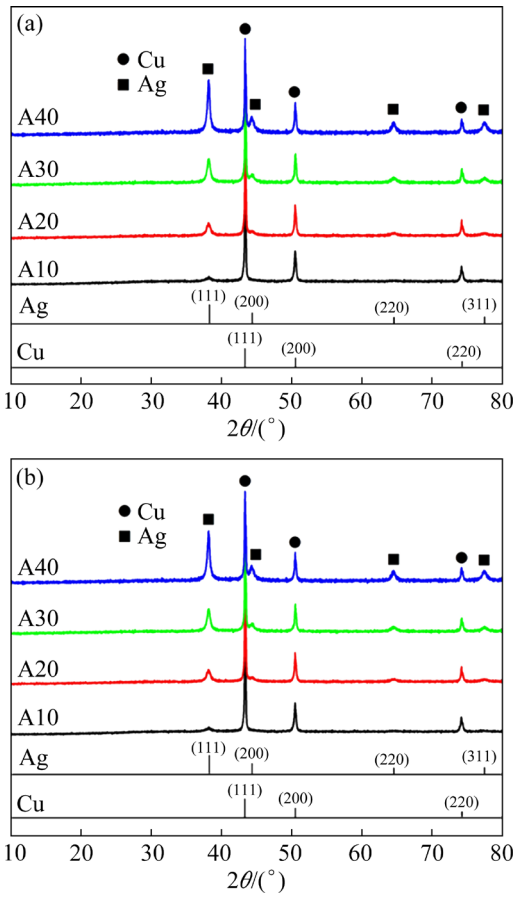

Fig. 6 XRD patterns of initial (a) and surface-modified (b) submicron Ag-coated Cu particles with different Ag contents

of ligands. The intensities of the peaks attributed to Cu and Ag also did not change after surface modification, confirming that the particles remained stable even during ultrasonic treatment.

Figure 7 shows the FT-IR spectra of pure stearic acid and the initial and surface-modified submicron Cu@Ag particles of A40. For the initial Cu@Ag particles, no peaks were observed at any wavenumber, and the upward peaks observed at 3200−3700 and 1600−1700 cm^{-1} in all cases originated from the H_2O molecules adsorbed during the pretreatment process of the sample for measurement. In the case of pure stearic acid and surface-modified Cu@Ag particles, peaks arising from the symmetrical stretching vibration of the carbonyl groups (C═O) present in the carboxylates were detected at 1705 and 1585 cm^{-1}, respectively, indicating that carboxylate ligands were formed on the surface after surface modification [39,40]. In addition, the negative shift of the peak attributed to υ_s (C═O) is owing to the decrease in stretching force constant caused by the coordination bond formed between the O atoms of carboxylate ligands and Ag atoms on the surface of the Ag shell [41,42]. For surface-modified particles, in addition to the peak owing to υ_s (C═O), asymmetrical stretching vibration of CH_3, asymmetrical and symmetrical stretching vibration of CH_2, asymmetrical stretching vibration of COO^-, bending vibration of CH_2, symmetrical stretching vibration of COO^-, and rocking vibration of CH_2 were detected at 2958, 2916, 2850, 1470, 1443, 1412, and 719 cm^{-1}, respectively [43,44]. All these peaks are attributed to the functional groups present in the stearic acid molecules, including carboxylates and alkyl chains; thus, it was verified that the carboxylate ligands were bonded to the Ag shell.

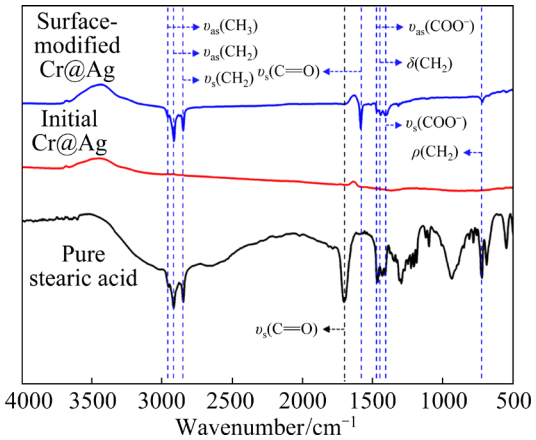

Fig. 7 FT-IR spectra of pure stearic acid, and initial and surface-modified submicron Ag-coated Cu particles of A40

Figure 8 shows the XPS Ag 3d spectra of the initial and surface-modified Cu@Ag particles. For the initial Cu@Ag particles, an Ag^0 peak corresponding to the Ag shell was detected at 368.2 eV. However, for the surface-modified particles, the Ag^0 peaks were detected at 368.7 eV for all four particles, exhibiting a chemical shift of 0.5 eV. This is due to the decrease in the shielding effect because the highly electronegative O atom of the carboxylate ligands attracts electrons from the Ag atom when forming coordination bonds with the Ag shell [45,46]. Therefore, it was confirmed that carboxylate ligands were formed after surface modification, similar to the FT-IR analysis results (Fig. 7). In addition, no differences in the chemical shift with different Ag contents were observed, and we concluded that the effectiveness of the surface modification dose not vary depending on the thickness of the Ag shell.

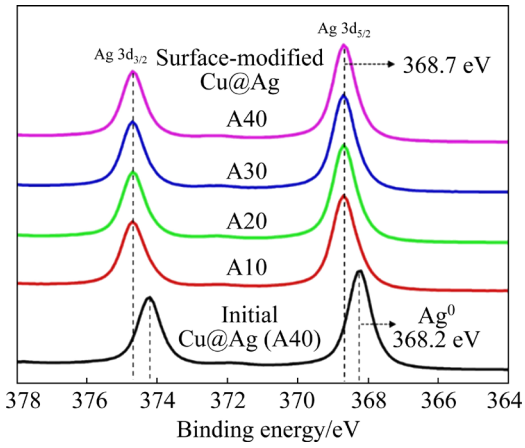

Fig. 8 XPS Ag 3d spectra of initial A40 and surface-modified submicron Ag-coated Cu particles with different Ag contents

3.3 Thermal properties of Cu@Ag pastes

Figure 9 shows the TG−DTA curves of the pastes containing initial and surface-modified submicron Cu@Ag particles with different Ag contents during dynamic heating in air. For all pastes, a mass loss of ~25% occurred in the temperature range of 180−260 °C owing to the evaporation of a solvent, which is approximately the same as the mass of the solvent mixed with the powder during paste preparation. Thereafter, the mass remained constant until the temperature increased

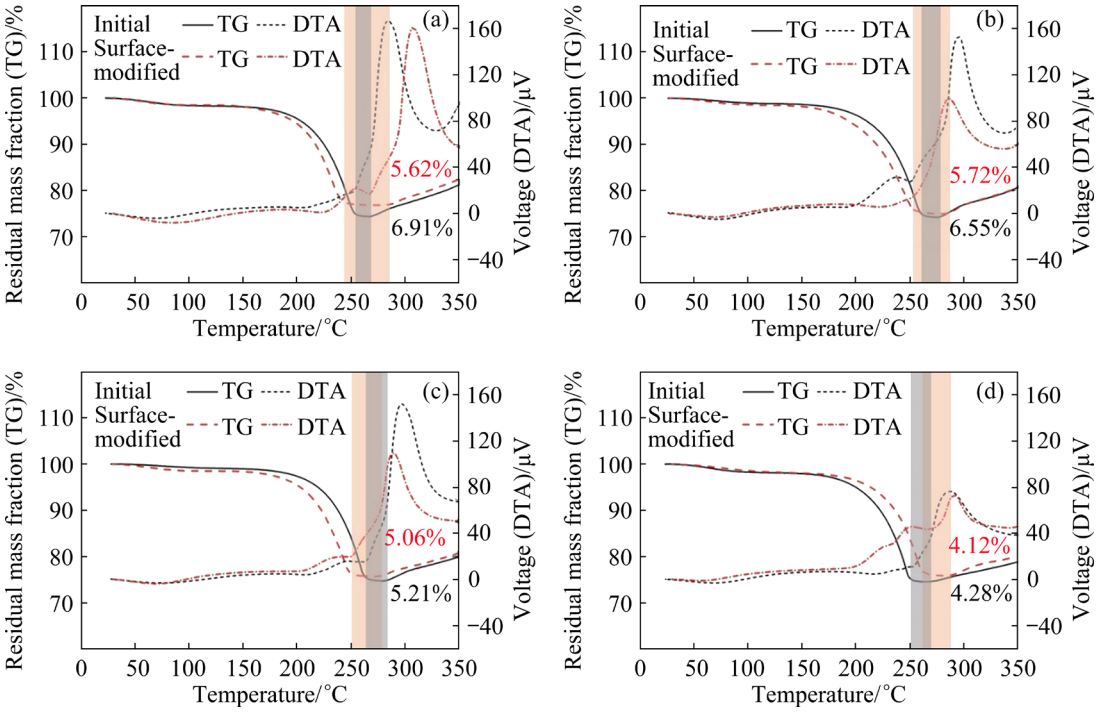

Fig. 9 TG−DTA curves of pastes containing initial and surface-modified submicron Ag-coated Cu particles with different Ag contents of 10 wt.% (a), 20 wt.% (b), 30 wt.% (c), and 40 wt.% (d)

by 20−40 °C, and then gradually increased because of the oxidation caused by the out-diffusion of core Cu and dewetting of Ag shell. In the case of initial particles, mass gains owing to oxidation began when the temperature increased by ~20 °C after solvent evaporation, but in the case of surface-modified particles, the mass gains did not occur until the temperature increased by ~40 °C. This is owing to the decrease in surface energy and concurrent suppression of Ag dewetting after surface modification; thus, the out-diffusion and exposure of the core Cu to air can be delayed. The mass gain at 350 °C decreased with increasing Ag content regardless of surface modification. The mass gains were 6.91%, 6.55%, 5.21%, and 4.28% for initial A10, A20, A30, and A40, respectively, which is owing to not only an increase in time for core Cu to diffuse out but also a delay in dewetting of abundant Ag with increasing thickness of Ag shell. Furthermore, for surface-modified A10, A20, A30, and A40, the mass gains at 350 °C were 5.62%, 5.72%, 5.06%, and 4.12%, respectively. These values were lower than those of the initial particles because an organometallic surface with relatively low energy effectively suppressed the Ag dewetting and delayed oxidation of the core Cu. This implies that the Ag shell maintains its conformal thickness for a longer time, even at relatively high temperatures, thereby reducing the out-diffusion rate of the core Cu. In addition, the difference in mass gain between the initial and surface-modified Cu@Ag particles varied with the Ag content, and the values were 1.29%, 0.83%, 0.15%, and 0.16% for A10, A20, A30, and A40, respectively. Among these, A10 exhibited the largest value, which was because the surface modification was the most effective in suppressing Ag dewetting in A10, which had the thinnest Ag shell (Fig. 9(a)). For all the pastes, large exothermic peaks accompanied by mass gain due to Cu oxidation were observed, and their sizes decreased with increasing Ag content and after surface modification. These results indicated a decrease in the relative degree of oxidation, which was consistent with the trends observed in the mass gain.

Figure 10 shows the TG−DTA curve of the surface-modified A40 during isothermal heating at 250 °C in a nitrogen atmosphere. The sample was heated to 250 °C at a heating rate of 30 °C/min and maintained for 20 min. The temperature reached 250 °C after heating for 8 min, where mass loss began simultaneously, and the rate significantly decreased after ~11 min. Subsequently, a slight

mass loss proceeded slowly, and the final mass loss after heating for 20 min was ~0.8%. The rapid mass loss from the point where the temperature reached 250 °C is owing to the removal of carboxylate ligands, and gaseous by-products such as H_2O, CO_2, H_2, C_2H_4, and CH_4 are formed because of the thermal decomposition of stearic acid in an inert atmosphere [47−49]. Most ligands were removed after ~5 min from the time when the temperature reached 250 °C, and the subsequent slight mass loss is due to the gradual removal of residual ligands that were not completely removed. The small and broad exothermic peak accompanied with the mass loss was attributed to sintering between the particles after pyrolysis of the carboxylate ligands.

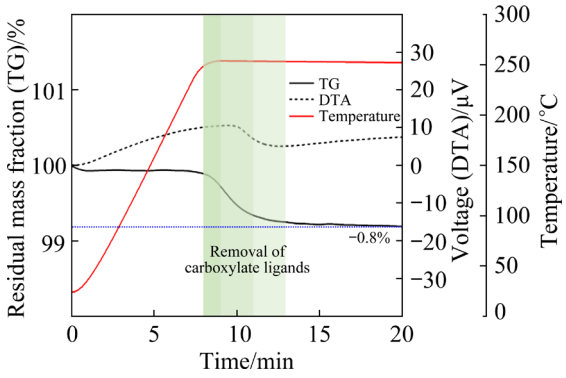

Fig. 10 TG−DTA curves of surface-modified A40 during isothermal heating for 20 min to 250 °C in nitrogen atmosphere

3.4 Sintering behavior using submicron Cu@Ag pastes

Figure 11 shows the electrical resistivities of films containing the initial and surface-modified submicron Cu@Ag particles with different Ag contents after sintering at 250 °C in a nitrogen atmosphere as a function of the sintering time. Electrical resistivity was calculated by multiplying the measured resistance value by a correction factor of 3.5098, which was determined by considering the temperature during the measurement and diameter of the film and then multiplying it by the thickness of the sintered film [50]. Because the out-diffusion of the core Cu barely occurs during sintering in a nitrogen atmosphere, copper oxide, which severely deteriorates sinterability, is not formed. Therefore, the resistivities decreased with increasing sintering time for all particles. When the sintering time was <3 min, the resistivities of the surface-modified Cu@Ag particles were higher

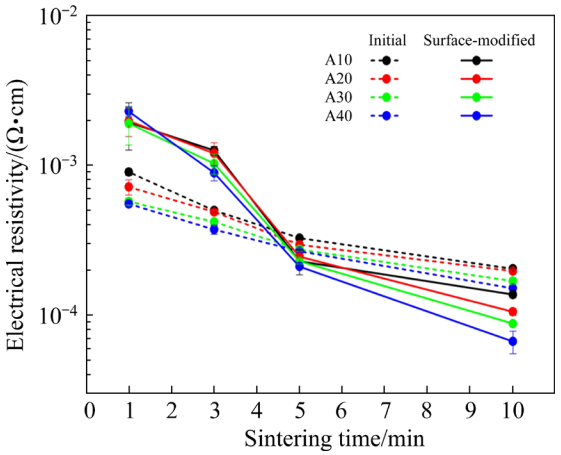

Fig. 11 Electrical resistivities of films containing initial and surface-modified submicron Ag-coated Cu particles with different Ag contents after sintering for 1−10 min at 250 °C in nitrogen atmosphere

than those of the initial particles, which was contrary to expectations. Based on the results shown in Fig. 10, this was probably because the ligands on the surface were removed incompletely when heated at 250 °C for 3 min, and they hindered the sintering between particles. In particular, nearly no trend or difference in the resistivity values was observed with different Ag contents when sintered for 1 min, such as A40, with the highest Ag content exhibiting the highest value. This is because the Ag content and thickness of the Ag shell are not dominant factors affecting sinterability, which is attributed to the residual ligands on the surface. For the initial Cu@Ag particles, the resistivities decreased with increasing Ag content, regardless of the sintering time. However, when the sintering time was 5 min, most ligands were removed and sintering proceeded; thus, the electrical resistivity values of the surface-modified particles were lower than those of the initial particles. When the sintering time was 10 min, the difference between the resistivity values before and after surface modification was larger than that after sintering for 5 min. This was owing to the suppression of Ag dewetting by the organometallic surface. While the Ag shell was maintained at a uniform thickness, the interparticle sinterability rapidly increased owing to the increase in the contact area of Ag. Therefore, in the case of surface-modified particles, the thickness of the Ag shell, that is, the absolute amount of Ag, considerably affects sinterability. Thus, large differences in resistivity values were observed with

different Ag contents when sintered for 10 min. In particular, while initial A40 exhibited the electrical resistivity value of $1.51\times10^{-4}\,\Omega\cdot$cm, that of the surface-modified A40 was $6.67\times10^{-5}\,\Omega\cdot$cm, which is less than half of that of initial particles. Therefore, surface modification using stearic acid effectively suppressed Ag dewetting and enhanced sinterability.

Figure 12 shows BSE images of the cross-sectional microstructure of films containing initial and surface-modified submicron Cu@Ag particles with different Ag contents after sintering at 250 °C for 10 min in a nitrogen atmosphere. The ratio of Ag which appears as a relatively bright region in the microstructure, increased with increasing Ag content. For the initial Cu@Ag particles, the dewetted Ag and neighboring particles formed sintered bodies earlier than the core Cu. The sintered bodies have different shapes, such as Ag filling up the spaces between three or more Cu particles, agglomerated Ag with a large amount on one side of the particle, and Ag bridges connecting two Cu particles. Because Ag exhibits more excellent sinterability even at relatively low temperatures than Cu, it can be sintered at 250 °C, but Cu undergoes rapid sintering only at temperatures >300 °C, owing to its self-diffusion. Therefore, structures where bare Cu particles were connected by sintering because of Ag dewetting were hardly observed, and the necks between particles by sintering were mainly formed by dewetted Ag. Consequently, it was confirmed that the contact area between the particles decreased and sinterability was reduced owing to the uneven distribution of Ag attributed to the severely agglomerated Ag particles, which was exacerbated with increasing Ag content. By contrast, for the surface-modified Cu@Ag particles, Ag dewetting was effectively suppressed, and a uniform distribution of Ag was maintained even after sintering for 10 min. Accordingly, necks and sintered body networks were more densely formed through sufficient contact between the Ag shells. The effectiveness of Ag dewetting suppression by surface modification was most prominent in A10, which is consistent with the TG−DTA results shown in Fig. 9. However, no significant improvement was observed in the electrical resistivity of A10 after surface modification compared to that of A40, as shown in Fig. 11, because the absolute amount of Ag was low and insufficient to form dense sintered bodies and networks. Considering these results, the application of low-Ag-content Cu@Ag particles is expected to expand through follow-up research.

4 Conclusions

(1) Changes in the surface morphology and bonding states of the Cu@Ag particles after surface modification were confirmed using SEM, FT-IR, and XPS.

(2) The effect of surface modification on suppressing Ag dewetting was confirmed by TG−DTA results: A decrease in mass gain at 350 °C, the shrunk size of the exothermic peak, and a delay in the onset temperature of mass gain by the oxidation of core Cu. The effect was the greatest in A10.

(3) The electrical resistivities of the sintered films containing surface-modified Cu@Ag particles were lower than those of the initial Cu@Ag particles

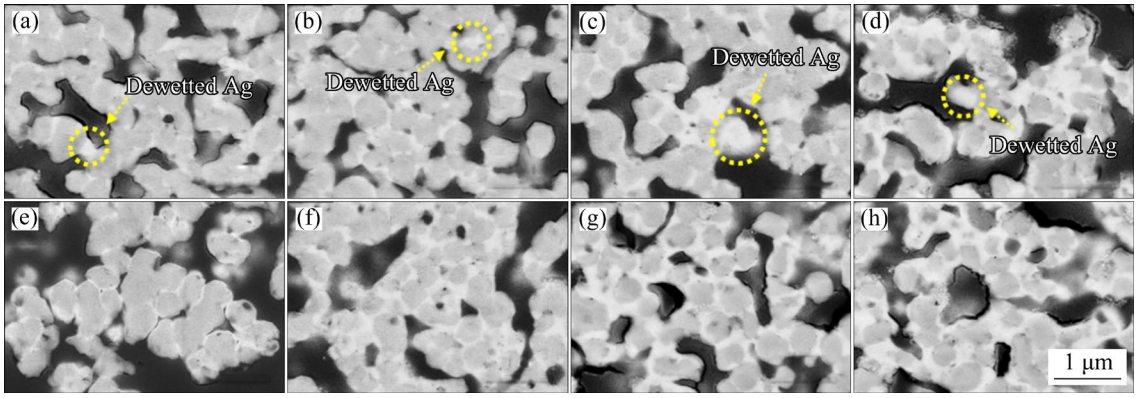

Fig. 12 Cross-sectional BSE images of films containing initial (a−d) and surface-modified (e−h) submicron Cu@Ag particles with different Ag contents of 10 wt.% (a, e), 20 wt.% (b, f), 30 wt.% (c, g), and 40 wt.% (d, h) after sintering at 250 °C for 10 min in nitrogen atmosphere

when the sintering time was >5 min. In particular, because the Ag content played a more dominant role in the resistivity than the effectiveness of surface modification, A40 showed the biggest difference in resistivity values after surface modification; surface-modified particles exhibited a resistivity of $6.67\times10^{-5}\,\Omega\cdot$cm when sintered for 10 min, which is less than half of that of initial particles ($1.51\times10^{-4}\,\Omega\cdot$cm). Therefore, the organometallic surface formed by stearic acid and the Ag shell effectively suppressed Ag dewetting, which increased the contact area between the Ag shells and improved the sinterability.

CRediT authorship contribution statement

Yeong-Jung KIM: Methodology, Investigation, Data curation, Formal analysis, Writing – Original draft, Review & editing; **Yong-Sung EOM** and **Kwang-Seong CHOI:** Conceptualization, Methodology, Investigation; **Jong-Hyun LEE:** Conceptualization, Methodology, Investigation, Formal analysis, Resources, Supervision, Funding acquisition, Writing – Original draft, Review & editing.

Declaration of competing interest

The authors declare that they have no known competing financial interests or personal relationships that could have appeared to influence the work reported in this paper.

Acknowledgments

This work was supported by the National Research Foundation of Korea (NRF) grant funded by the Korea government (MSIT) (No. 2021R1A2C1007400). This research was supported, partly, by the National R&D Program through the National Research Foundation of Korea (NRF) funded by the Ministry of Science and ICT (Nos. NRF-2020M3H4A3106383, NRF-2020M3H4A3081764) and was supported, partly, by ETRI (No. 21YB1610). This work was also supported by a Korea Institute for Advancement of Technology (KIAT) grant funded by the Korea Government (MOTIE) (No. P0008458, HRD Program for Industrial Innovation).

References

[1] CHANG Y, WANG D Y, TAI Y L, YANG Z G. Preparation, characterization and reaction mechanism of a novel silver-organic conductive ink [J]. Journal of Materials Chemistry, 2012, 22: 25296−25301.

[2] ZHU Y M, CHEN X, CHANG Y, YANG Z G. Fabrication of double-sided FPC by hydrolyzing-doping-plating additive process [J]. Journal of the Electrochemical Society, 2018, 165: 494−499.

[3] SHUKLA D, LIU Y, ZHU Y. Eco-friendly screen printing of silver nanowires for flexible and stretchable electronics [J]. Nanoscale, 2023, 15: 2767−2778.

[4] FENG J X, ZHANG Z Y, LIU J B, SHAO M, ZHOU Y. A novel resistive anode using a germanium film for micromegas detectors [J]. Nuclear Instruments and Methods in Physics Research Section A: Accelerators, Spectrometers, Detectors and Associated Equipment, 2022, 1031: 166595−166599.

[5] GOH G L, ZHANG H N, CHONG T H, YEONG W Y. 3D printing of multilayered and multimaterial electronics: A review [J]. Advanced Electronic Materials, 2021, 7: 2100445−2100472.

[6] SONG S M, CHO S M. Copper ion inks capable of screen printing and intense pulsed-light sintering on PET substrates [J]. ACS Applied Electronic Materials, 2022, 4: 1882−1890.

[7] KANG H, SOWADE E, BAUMANN R R. Direct intense pulsed light sintering of inkjet-printed copper oxide layers within six milliseconds [J]. ACS Applied Materials & Interfaces, 2014, 6: 1682−1687.

[8] QIN G, WATANABE A, TSUKAMOTO H, YONEZAWA T. Copper film prepared from copper fine particle paste by laser sintering at room temperature: Influences of sintering atmosphere on the morphology and resistivity [J]. Japanese Journal of Applied Physics, 2014, 53: 096501−096509.

[9] ZHAO P B, HUANG J, NAN J Z, LIU D C, MENG F B. Laser sintering process optimization of microstrip antenna fabricated by inkjet printing with silver-based MOD ink [J]. Journal of Materials Processing Technology, 2020, 275: 116347−116361.

[10] NIITTYNEN J, ABBEL R, MÄNTYSALO M, PERELAER J, SCHUBERT U S, LUPO D. Alternative sintering methods compared to conventional thermal sintering for inkjet printed silver nanoparticle ink [J]. Thin Solid Films, 2014, 556: 452−459.

[11] PERELAER J, ABBEL R, WÜNSCHER S, JANI R, van LAMMEREN T V, SCHUBERT U S. Roll-to-roll compatible sintering of inkjet printed features by photonic and microwave exposure: From non-conductive ink to 40% bulk silver conductivity in less than 15 seconds [J]. Advanced Materials, 2012, 24: 2620−2625.

[12] KAMYSHNY A, MAGDASSI S. Conductive nanomaterials for printed electronics [J]. Small, 2014, 10: 3515−3535.

[13] SHEN W, ZHANG X, HUANG Q, XU Q, SONG W. Preparation of solid silver nanoparticles for inkjet printed flexible electronics with high conductivity [J]. Nanoscale, 2014, 6: 1622−1628.

[14] KIM I, KIM J. The effect of reduction atmospheres on the sintering behaviors of inkjet-printed Cu interconnectors [J]. Journal of Applied Physics, 2010, 108: 102807−102811.

[15] WU X, SHAO S, CHEN Z, CUI Z. Printed highly conductive Cu films with strong adhesion enabled by low-energy photonic sintering on low-Tg flexible plastic substrate [J]. Nanotechnology, 2017, 28: 035203−035211.

[16] KAMYSHNY A, MAGDASSI S. Metal-based inkjet inks for printed electronics [J]. The Open Applied Physics Journal, 2011, 4: 19−36.

[17] STEWART I E, KIM M J, WILEY B J. Effect of morphology on the electrical resistivity of silver nanostructure films [J]. ACS Applied Materials & Interfaces, 2017, 9: 1870−1876.

[18] LEE C, KIM N R, KOO J, LEE Y J, LEE H M. Cu−Ag core-shell nanoparticles with enhanced oxidation stability for printed electronics [J]. Nanotechnology, 2015, 26: 455601−455609.

[19] XU X R, LUO X J, ZHUANG H R, LI W L, ZHANG B L. Electroless silver coating on fine copper powder and its effects on oxidation resistance [J]. Materials Letters, 2003, 57: 3987−3991.

[20] YANG G N, ZOU Q Y, WANG P Y, LAI H, LAI T Q, ZENG X, LI Z, LUO J, ZHANG Y Y, CUI C Q. Towards understanding the facile synthesis of well-covered Cu−Ag core-shell nanoparticles from a complexing model [J]. Journal of Alloys and Compounds, 2021, 874: 159900−159909.

[21] YANG G N, WANG P Y, LIU Y, LU S Z, LUO B, LAI T, TA S W, LIN T, LUO J Y, ZHANG Y, CUI C Q. Effect of Ag coating on the oxidation resistance, sintering properties, and migration resistance of Cu particles [J]. Journal of Alloys and Compounds, 2022, 923: 166271−166281.

[22] ZHANG R W, LIN W, LAWRENCE K, WONG C P. Highly reliable, low cost, isotropically conductive adhesives filled with Ag-coated Cu flakes for electronic packaging applications [J]. International Journal of Adhesion and Adhesives, 2010, 30: 403−407.

[23] WU M, LIN B P, CAO Y, SONG J G, SUN Y, YANG H, ZHANG X Q. Preparation and sintering properties in air of silver-coated copper powders and pastes [J]. Journal of Materials Science: Materials in Electronics, 2013, 24: 4913−4918.

[24] LI W, LI W J, WANG M M, LIU G X, CHEN M F. Direct writing of stable Cu−Ag-based conductive patterns for flexible electronics [J]. RSC Advances, 2016, 6: 10670−10676.

[25] YU X, LI J J, SHI T L, CHENG C L, LIAO G L, FAN J H, LI T X, TANG Z R. A green approach of synthesizing of Cu-Ag core-shell nanoparticles and their sintering behavior for printed electronics [J]. Journal of Alloys and Compounds, 2017, 724: 365−372.

[26] HAJIBABAEI M, AMINI M M, ZENDEHDEL R, NASIRI M J, PEYMANI A. Synthesis, characterization and antibacterial activity of imidazole-functionalized Ag/MIL-101(Cr) [J]. Journal of Porous Materials, 2019, 26: 1721−1729.

[27] LOU X Y, BOADA R, VERDUGO V, SIMONELLI L, PÉREZ G, VALIENTE M. Decoupling the adsorption mechanisms of arsenate at molecular level on modified cube-shaped sponge loaded superparamagnetic iron oxide nanoparticles [J]. Journal of Environmental Sciences, 2022, 121: 1−12.

[28] PALANISAMY S, KARUPPIAH C, CHEN S M, EMMANUEL R, MUTHUKRISHNAN P, PRAKASH P. Direct electrochemistry of myoglobin at silver nanoparticles/ myoglobin biocomposite: Application for hydrogen peroxide sensing [J]. Sensors and Actuators B: Chemical, 2014, 202: 177−184.

[29] TOISAWA K, HAYASHI Y, TAKIZAWA H. Synthesis of highly concentrated Ag nanoparticles in a heterogeneous solid-liquid system under ultrasonic irradiation [J]. Materials Transactions, 2010, 51: 1764−1768.

[30] SHAHMORADI B, MALEKI A, BYRAPPA K. Photocatalytic degradation of amaranth and brilliant blue FCF dyes using in situ modified tungsten doped TiO_2 hybrid nanoparticles [J]. Catalysis Science & Technology, 2011, 1: 1216−1223.

[31] ZHANG S Y, QI X Q, YANG M, CAO Y, LIN T S, HE P, PAIK K W. A study on the resistivity and mechanical properties of modified nano-Ag coated Cu particles in electrically conductive adhesives [J]. Journal of Materials Science: Materials in Electronics, 2019, 30: 9171−9183.

[32] CHEN D P, ZHAO L, DIAO H W, ZHANG W B, WANG G, WANG W J. Low-temperature sintering properties of the screen-printed silver paste for a-Si:H/c-Si heterojunction solar cells [J]. Journal of Materials Science: Materials in Electronics, 2014, 25: 2657−2664.

[33] YANG X J, HE W, WANG S X, ZHOU G Y, TANG Y. Preparation of high-performance conductive ink with silver nanoparticles and nanoplates for fabricating conductive films [J]. Materials and Manufacturing Processes, 2012, 28: 1−4.

[34] LEE C H, CHOI E B, LEE J H. Characterization of novel high-speed die attachment method at 225 °C using submicrometer Ag-coated Cu particles [J]. Scripta Materialia, 2018, 150: 7−12.

[35] MUZIKANSKY A, NANIKASHVILI P, GRINBLAT J, ZITOUN D. Ag dewetting in Cu@Ag monodisperse core–shell nanoparticles [J]. The Journal of Physical Chemistry C, 2013, 117: 3093−3100.

[36] KIM S Y, CHOI E B, JOO D H, LEE J H. High-speed formation of a near-full-density bondline in sinter-bonding below 250 °C using 2 μm Cu particles coated with Ag [J]. Powder Metallurgy, 2020, 63: 367−380.

[37] KIM Y, CHOI E B, LEE J H. Surface modification of Ag-coated Cu particles using dicarboxylic acids to enhance the electrical conductivity of sintered films by suppressing dewetting in Ag shells [J]. Applied Surface Science, 2023, 640: 158326−158340.

[38] KAMAT G A, YAN C, OSOWIECKI W T, MORENO-HERNANDEZ I A, LEDENDECKER M, ALIVISATOS A P. Self-limiting shell formation in Cu@Ag core-shell nanocrystals during galvanic replacement [J]. The Journal of Physical Chemistry Letters, 2020, 11: 5318−5323.

[39] LI Q Q, BAO X G, SUN J E, CAI S, XIE Y, LIU Y, LIU J, XU G. Fabrication of superhydrophobic composite coating of hydroxyapatite/stearic acid on magnesium alloy and its corrosion resistance, antibacterial adhesion [J]. Journal of Materials Science, 2021, 56: 5233−5249.

[40] LEE S J, KIM K. Diffuse reflectance infrared spectra of stearic acid self-assembled on fine silver particles [J]. Vibrational Spectroscopy, 1998, 18: 187−201.

[41] AKYUZ S. The FT-IR spectra of pyrazinamide complexes of transition metal(II) tetracyanonickelate [J]. Journal of Molecular Structure, 2003, 651/652/653: 541−545.

[42] AKYUZ S, AKYUZ T. FT-IR spectroscopic investigations adsorption of pyrazinamide and 4-aminopyrimidine by clays [J]. Journal of Inclusion Phenomena and Macrocyclic

Chemistry, 2004, 48: 75−80.
[43] NGUYEN D M, VU T N, NGUYENTT M L, NGUYEN T D, THUC C N H, BUI Q B, COLIN J, PERRÉ P. Synergistic influences of stearic acid coating and recycled PET microfibers on the enhanced properties of composite materials [J]. Materials (Basel), 2020, 13: 1461−1476.
[44] MAO Y, DUAN Y, WANG K, XI L, DENG Q, WANG G, WANG S. Preparation of Ag nanoparticles coated with silver stearate for low-temperature sinter-bonding [J]. Journal of Electronic Materials, 2019, 48: 3336−3344.
[45] GUAY-BÉGIN A A, CHEVALLIER P, FAUCHER L, TURGEON S, FORTIN M A. Surface modification of gadolinium oxide thin films and nanoparticles using poly(ethylene glycol)-phosphate [J]. Langmuir, 2012, 28: 774−782.
[46] FENG N D, WANG Q, ZHENG A M, ZHANG Z F, FAN J, LIU S B, AMOUREUX J P, DENG F. Understanding the high photocatalytic activity of (B,Ag)-codoped TiO_2 under solar-light irradiation with XPS, solid-state NMR, and DFT calculations [J]. Journal of the American Chemical Society, 2013, 135: 1607−1616.
[47] JIN C Y, ZHOU L P, FU L C, ZHU J J, LI D Y. Synthesis and discharge performances of $NiCl_2$ by surface modification of carbon coating as cathode material of thermal battery [J]. Applied Surface Science, 2017, 402: 308−313.
[48] ZHANG Y, ZHANG C B, LI W J, XIAO Q P, JIAO F Y, XU S, LAN Y H, FU Y Z, SHU C M, CAO W G. Reaction mechanism of stearic acid pyrolysis via reactive molecular dynamics simulation and TG-IR technology [J]. Renewable Energy, 2023, 217: 119115−119125.
[49] BAUM M M, BECKER R M, LAPPAS A M, MOSS J A, APELIAN D, SAHA D, KAPINUS V A. Lubricant pyrolysis during sintering of powder metallurgy compacts [J]. Metallurgical and Materials Transactions B, 2004, 35: 381−392.
[50] SMITS F M. Measurement of sheet resistivities with the four-point probe [J]. The Bell System Technical Journal, 1958, 37: 711−718.

硬脂酸表面改性亚微米银包铜颗粒作为烧结浆料填料抑制银去润湿现象和提高烧结性能

Yeongjung KIM[1], Yong-Sung EOM[2], Kwang-Seong CHOI[2], Jong-Hyun LEE[1,3]

1. Department of Materials Science and Engineering, Seoul National University of Science and Technology, 232 Gongneung-ro, Nowon-gu, Seoul 01811, Korea;
2. Low-Carbon Integration Tech, Creative Research Section, ETRI, 218 Gajeong-ro, Yuseong-gu, Daejeon 34129, Korea;
3. Materials Research Institute for Future Convergence, Seoul National University of Science and Technology, 232 Gongneung-ro, Nowon-gu, Seoul 01811, Korea

摘　要：制备了银质量含量分数为 10%、20%、30%和 40%的 4 种亚微米级银包铜颗粒，作为烧结浆料的填料。对这 4 种颗粒(按银含量递增的顺序命名为 A10、A20、A30 和 A40)进行硬脂酸表面改性处理，以抑制银壳的去润湿现象并提升烧结性能。将表面改性的颗粒与多元醇基溶剂混合，制备成无树脂型浆料，然后通过丝网印刷将浆料涂覆于载玻片上，并在氮气气氛、250 ℃下烧结 1~10 min，形成电极。采用四探针法测量烧结薄膜的电阻率随烧结时间的变化。经表面改性的 4 种 Cu@Ag 颗粒，无论银含量高低，电阻率均降低，特别是银含量最高的 A40 颗粒，烧结 10 min 后，初始颗粒和表面改性颗粒的电阻率分别为 1.51×10^{-4} 和 6.67×10^{-5} Ω·cm，二者差值最大。结果表明，采用硬脂酸对亚微米级 Cu@Ag 颗粒进行表面改性能有效抑制其银壳的去润湿现象，并显著改善其烧结性能。

关键词：亚微米银包铜颗粒；烧结；去润湿；表面改性；硬脂酸；电阻率

(Edited by Wei-ping CHEN)